Journal of Molecular Graphics and Modelling 45 (2013) 38–44

Contents lists available at ScienceDirect

Journal of Molecular Graphics and Modelling

journal homepage: www.elsevier.com/locate/JMGM

Elucidating binding modes of zuonin A enantiomers to JNK1 via in silico methods

Daniel W. Dykstra[a,c], Kevin N. Dalby[b,c], Pengyu Ren[a,*]

[a] Department of Biomedical Engineering, University of Texas at Austin, TX 78712, USA
[b] Division of Medicinal Chemistry, University of Texas at Austin, TX 78712, USA
[c] Department of Biochemistry, University of Texas at Austin, TX 78712, USA

ARTICLE INFO

Article history:
Received 4 June 2013
Received in revised form 24 July 2013
Accepted 6 August 2013
Available online 16 August 2013

Keywords:
Kinase
Non-ATP competitive inhibitor
Docking
Molecular dynamics
JNK
MAPK

ABSTRACT

Aberrant c-Jun N-terminal kinase (JNK) signaling is associated with a number of diseases, including neurological conditions and cancer. Enantiomers of the lignan zuonin A, (−)-zuonin A and (+)-zuonin A bind isoforms of JNK with similar affinity and disrupt protein-protein interactions at JNK's D-recruitment site. Thus, they are of interest as lead non-ATP competitive inhibitors of the JNKs. While (−)-zuonin A inhibits the activity of JNK toward c-Jun by 80% when saturating, (+)-zuonin A only inhibits by 15%. Molecular docking and molecular dynamics simulations were performed to gain a better understanding of how these inhibitors interact with JNK. The results of this study provide new insight into potential binding modes for (−)-zuonin A and suggest that (−)-zuonin A interacts with JNK via an induced fit mechanism near the highly conserved φ_A-X-φ_B recognition site. Binding of (+)-zuonin A to JNK displays no such dynamic feature. The different binding modes may help explain differences in the inhibitory properties of the enantiomers although further experimental work would be necessary to fully confirm this interpretation.

1. Introduction

c-Jun N-terminal kinases (JNKs) are members of the MAP kinase family and play an integral role in eukaryotic cellular stress response mechanisms. JNK is encoded by genes *Jnk1*, *Jnk2*, and *Jnk3* and have 10 different splice variants. While JNK1 and JNK2 are ubiquitously expressed throughout the body, JNK3 is predominately localized to the brain, testis and heart.

All isoforms are activated by dual phosphorylation of the Thr-Pro-Tyr motif located on the activation loop of the enzyme. The tyrosine and threonine residues are phosphorylated by upstream kinases MKK4 and MKK7 respectively [1]. Like other MAP kinases, JNKs make use of a D-recruitment site (DRS) docking region to recruit, orient, and discriminate between activators, regulators, and substrates. The DRS targets proteins and peptides containing a D-site motif via a negatively charged common docking (CD) domain and a hydrophobic groove. The consensus sequence for the D-site motif is $\theta_{(1-3)}$–$X_{(0-5)}$–φ_L–$X_{(1-2)}$–φ_A–X–φ_B, where X is any amino acid, θ represents positively charged amino acids, and φ are hydrophobic residues. Successful binding to this region helps align the two proteins and increases the likelihood for the desired catalytic reaction [2].

Aberrant JNK signaling can result in two main forms of disease in humans: (1) neurological, coronary, hepatobiliary, and respiratory diseases and (2) autoimmune, inflammatory, and cancer conditions. JNKs play a vital role in proper brain/neurological development. Single knockout studies of any JNK isoform, in addition to *Jnk1*/*Jnk3* and *Jnk2*/*Jnk3* double knockouts, had no deleterious effects on mouse development. However, the *Jnk1*/*Jnk2* double knockout resulted in early embryonic termination due to unregulated apoptosis of neuronal cells in the brain. This suggests that JNK1 and JNK2 may have some redundant functions. Contrary to their similar function in brain development, JNK1 and JNK2 appear to have separate roles in fibroblast proliferation and the progression of certain forms of cancer. Studies have shown that upregulation of JNK1 increases c-Jun phosphorylation and activation resulting in cellular proliferation, while the inverse is true for JNK2. The diverse roles of JNKs in human pathogenesis make it a desirable drug target, however, finding the appropriate specificity amongst other kinases, let alone the JNK isoforms, has been a challenge [3].

Two main strategies have been employed for the development of JNK inhibitors. ATP competitive inhibitors target the ATP binding pocket, as the name suggests, while non-ATP competitive inhibitors bind to the D-recruitment site and disrupt target substrate binding. One successful ATP competitive inhibitor, SP600125, has been proven to be effective at inhibiting JNK in both cell culture as well as mouse models. However, targeting the ATP binding site comes at the cost of reduced specificity due to the conserved nature and

* Corresponding author.
E-mail address: pren@mail.utexas.edu (P. Ren).

1093-3263/$ – see front matter © 2013 Elsevier Inc. All rights reserved.
http://dx.doi.org/10.1016/j.jmgm.2013.08.008

abundance of ATP binding pockets [4]. In addition, ATP competitive inhibitors must compete with high concentrations of intracellular ATP, which vary from 1 to 10 mM.

For these reasons, there has been interest in developing non-ATP competitive inhibitors. A JNK interacting protein-1 (JIP1) peptide fragment known to interact with the JNK D-recruitment site was able to selectively inhibit JNK over other similar MAP kinases, such as ERK2 and p38. Unfortunately, the large number of degrees of freedom of the peptide backbone and issues with bioavailability makes a peptide a somewhat undesirable lead compound. To combat this issue, a library of small molecules was screened to reveal compounds capable of disrupting the JIP1 and JNK1 interaction. One potential lead discovered in this screen was BI-78D3. BI-78D3 confirmed that the concept of targeting the DRS using small molecules could potentially be effective by inhibiting the phosphorylation of JNK1 substrates in a dose dependent manner [5].

In order to expand on the number of non-ATP competitive inhibitor scaffolds, we previously performed a virtual screen to compare BI-78D3 to other compounds based on three-dimensional shape and electrostatic similarities [6]. One compound of interest isolated from this study was the lignan (−)-zuonin A, Fig. 1A, which has a 100-fold greater selectivity toward inhibiting JNK–protein interactions over ERK2 and p38 MAPKα. To the best of our knowledge, the zuonin is perhaps the most specific non-ATP competitive MAP kinase inhibitors reported to date.

An interesting observation regarding (−)-zuonin A and its enantiomer, (+)-zuonin A, is that both have similar affinities for JNK1. However, at saturating concentrations, (−)-zuonin A Exhibits 80% of the theoretical maximal amount of inhibition, whereas (+)-zuonin A only exhibits about 15%. This information suggests that the two zuonin A enantiomers interact with JNK differently [7].

A potential binding mode for (−)-zuonin A to JNK1 was previously determined using a combination of molecular docking and molecular dynamics simulations. In the present study, we performed more extensive MD simulations of both (−)-zuonin A and (+)-zuonin A/JNK1 complexes to gain a better understanding of each enantiomer's binding mode and examine the specific interactions between the inhibitors and JNK1.

2. Methods

2.1. In silico representations of JNK1 and zuonin A

The dephosphorylated JNK1 structure used was previously generated by adding back missing amino acid residues to the crystal structure of the JNK1–JIP1 peptide complex (PDB ID: 1UKH) [4] using the homology software Modeler9v5 [8]. Missing residues were far enough away from the proposed binding sites that they do not affect the docking results. Zuonin enantiomers were drawn using MarvinSketch and converted to 3D coordinates.

2.2. Molecular docking

Docking experiments were performed using Genetic Optimization for Ligand Docking (GOLD) software provided by the Cambridge Crystallographic Data Centre (CCDC) [9]. Both zuonin A enantiomers were docked 100 times into 10 different regions along the JNK–JIP1 interface yielding 1000 potential poses. The regions were defined as all JNK atoms within a 16 Å radius of each JIP1 α-carbon to accommodate the approximate width of zuonin (∼14 Å). Each docking began with an initial population of 200 members divided onto 5 islands. Crossover events were controlled using a niche size of 2 and a selection pressure of 1.1. The quality of fit for each pose was calculated using the Chemscore fitness function with the default parameters supplied by CCDC.

All docking poses were combined and clustered based on their RMSD calculated using GoldMine [9]. The highest scoring pose in each cluster was selected for the subsequent molecular dynamics simulation.

2.3. Molecular dynamics simulations

Gaussian09 quantum mechanics software was used to optimize the 3D structures of zuonin molecules [10]. The atomic charges were determined using the Merz–Singh–Kollman scheme [11,12]. All calculations were performed using the Hartree–Fock/6-31G* basis set. The optimized structures were converted to Amber parameter and coordinate files using the antechamber and LEaP modules of Amber12 and the General Amber Force Field (GAFF) [13].

The topology and coordinate files for the zuonin–JNK1 complexes were created with LEaP using the ff99SB force field in conjunction with the previously generated parameter, coordinate and library files for zuonin. A set of topology and coordinate files were also created for the solvated system which consisted of a truncated octahedral TIP3P water box that extended 8 Å from the enzyme's surface and added 4 Na^+ counterions to balance the overall charge.

All minimization and MD equilibration steps were executed using the Sander module of Amber12 while production runs were performed using the PMEMD (Particle Mesh Ewald Molecular Dynamics) module. To remove any potential bad contacts, each system was minimized while holding the protein backbone rigid until it converged to less than 0.001 kcal/mole Å. The steepest descent algorithm was used for the first 500 steps followed by 500 cycles of the conjugate gradient method.

The system was equilibrated using a two-step process. First, a 200 ps NVT simulation was performed using a 2.0 fs integration timestep. The system was heated from 0 K to 300 K during the first 80 ps and held constant for the remainder of the simulation. A second 1 ns NPT equilibration step was executed at 1 bar to equilibrate the size of the system. In both steps, all backbone atoms present in the original crystal structure were restrained while all other atoms were allowed to move freely.

An 8 ns trajectory was then acquired for each production run. A total of 28 simulation runs were performed for both zuonin A enantiomers at various poses (14 for (−)-zuonin A and 14 for (+)-zuonin A). The conditions of this step were the same as the second equilibration step except all backbone restraints were removed.

For all MD simulations a Langevin thermostat was used to regulate the system's temperature, all covalent hydrogen bond lengths were constrained using the SHAKE algorithm, and a 10 Å cutoff was used for van der Waals interactions and Particle-Mesh-Ewald (PME) [14] for electrostatics.

2.4. Binding free energy via MM-GBSA

The Molecular Mechanics-Generalized Born Surface Area (MM-GBSA) implicit solvent method was used to estimate the free energy difference between the bound and unbound states of zuonin A to JNK1. This method estimates the change in free energy of ligand binding in a solvated system by calculating the solvation energies of JNK1 and zuonin A and subtracting them from the solvation energy of the complex and their binding free energy in vacuum:

$$\Delta G^0_{\text{Binding,solv}} = \Delta G^0_{\text{Solv,Complex}} + \Delta G^0_{\text{Binding,Vac}} + (\Delta G^0_{\text{Solv,Receptor}} + \Delta G^0_{\text{Solv,Ligand}}) \quad (1)$$

Solvation free energies, ΔG_{Solv}, are the sum of the solvation energy of the polar contributions, $\Delta G_{\text{Solv,polar}}$, as determined by

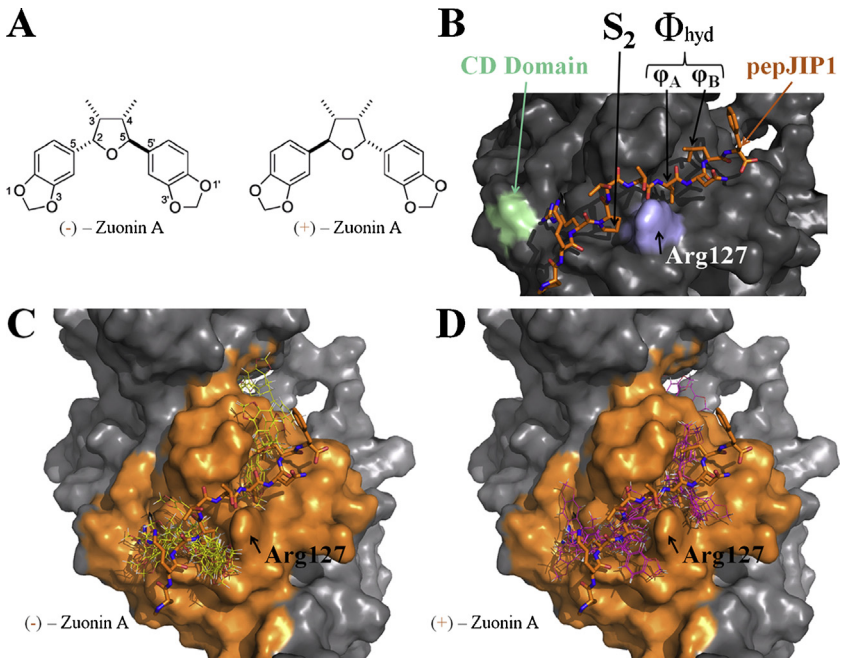

Fig. 1. (A) Chemical structure of zuonin A enantiomers. (B) Key features of JIP1 and JNK1 binding interactions. The two major binding regions for both zuonin enantiomers are denoted as S_2 and Φ_{hyd}. Docking Results for (C) (−)-zuonin A and (D) (+)-zuonin A superimposed with pepJIP1 on JNK1. The orange region is made up of JNK1 atoms within an 8 Å radius of each α-carbon.

the Generalized Born method [15], and the solvation energy of the non-polar portion, $\Delta G_{Solv,nonpolar}$, was calculated using the surface area of the molecule.

$$\Delta G_{Solv} = \Delta G_{Solv,polar} + \Delta G_{Solv,non-polar} \quad (2)$$

The binding free energy in a vacuum, $\Delta G_{Binding,Vac}$, is simply the sum of the change in enthalpy, $\Delta U_{MM,Vac}$, and entropy, $T\Delta S$, terms going from their respective unbound states to complex in the absence of solvent.

$$\Delta G_{Binding,Vac} = \Delta U_{MM,VAC} - T\Delta S \quad (3)$$

Thus, the solvated binding free energy can be approximated by combining the previous equations to get:

$$\Delta G_{Binding,Solv} = \Delta U_{MM,Vac} + \Delta G_{GB} + \Delta G_{SA} - T\Delta S \quad (4)$$

where $\Delta U_{MM,Vac}$ is calculated using the molecular mechanics force field, ΔG_{GB} is the electrostatic (polar) solvation energy calculated using the Generalized-Born method, ΔG_{SA} is the nonpolar contributions to solvation energy based on the exposed surface area, and ΔS is the change in entropy which can be estimated using normal mode analysis and other methods.

The MD trajectories from each 8 ns production run were processed with the MMPBSA.py module of Amber12. Due to the time consuming nature and unreliable methods currently available for estimating the protein and ligand entropic contributions, it was assumed that the effect of entropy on binding was similar across all simulations since the molecules being compared were identical and binding to similar pockets.

3. Results and discussion

3.1. Molecular docking

The resulting poses from molecular docking for both zuonin enantiomers docked to the pepJIP1 binding site of JNK1 tended to cluster into two regions that are critical for JIP1 peptide binding; the hydrophobic region (Φ_{hyd}) to the upper right of R127 which contains the highly conserved φ_A–X–φ_B recognition site, and the region to the lower left of R127 is denoted as "site 2" or S_2, as described by Kaoud et al., Fig. 1B [6]. The S_2 is mainly defined by another hydrophobic pocket that is usually occupied by Pro158 of pepJIP1 (φ_A-2). RMSD cluster analysis revealed 14 unique binding poses for each zuonin A enantiomer yielding 28 total configurations. Of the 14 predicted poses generated for (−)-zuonin A, 3 were bound to the Φ_{hyd} region with the 1,3-benzodioxole ring located in the φ_A–X–φ_B recognition site, while the remaining 11 poses were localized to the S_2 region (Fig. 1C). The majority of (+)-zuonin A molecules were also predicted to bind to the S_2 site (9 out of 14). However, unlike (−)-zuonin A, the 5 poses in the Φ_{hyd} region occupied the φ_A–X–φ_B recognition site through the THF ring (Fig. 1D).

Overall, docking poses that aggregated in the S_2 pocket scored more favorably than those bound to Φ_{hyd}, as shown in Table 1. Decomposition of the contributions for each ligand revealed that conformations bound to S_2 had a greater contribution from hydrophobic interactions than those bound to the Φ_{hyd} pocket (Supplementary Table 1). The S_2 pocket is deeper in the crystal structure than Φ_{hyd}, thus enhancing its ability to shield zuonin A's

Table 1
Molecular docking scores (ChemScore) of (−)-zuonin A and (+)-zuonin A poses bound to JNK1 and their binding region.

(−)-Zuonin A			(+)-Zuonin A		
Pose #	ChemScore	Region	Pose #	ChemScore	Region
10	25.7	S_2	20	26.7	S_2
11	24.7	S_2	1	25.5	S_2
12	24.6	S_2	7	25.4	S_2
27	24.2	S_2	31	24.7	S_2
14	24.0	S_2	19	24.5	S_2
9	24.0	S_2	22	24.3	S_2
31	23.9	S_2	15	24.2	S_2
24	23.8	S_2	34	23.8	S_2
33	23.6	S_2	4	23.6	S_2
40	23.4	S_2	41	22.3	Φ_{hyd}
37	23.2	S_2	46	22.2	Φ_{hyd}
43	19.6	Φ_{hyd}	32	21.5	Φ_{hyd}
44	19.6	Φ_{hyd}	39	21.3	Φ_{hyd}
45	18.7	Φ_{hyd}	49	20.8	Φ_{hyd}

hydrophobic core. Pose **20** had the highest chemscore (26.7) for (+)-zuonin A. This pose was bound to the S_2 site and had the THF ring in close proximity to the proline site with both methyl groups extended into the pocket. The pose appears to be further stabilized by the stacking of one of its 1,3-benzodioxole rings between the groove formed by Arg127, Cys163, and Asp162 (Supplementary Figure 1A). This pose was quite similar to a (−)-zuonin A binding mode proposed by Kaoud et al. [7]. The highest scoring pose for (−)-zuonin A was pose **10** as shown in Table 1. This pose also interacted with the S_2 site and had a chemscore of 25.7. Unlike (+)-zuonin A, pose **10** buried one of its 1,3-benzodioxole rings into the proline pocket and oriented itself in the opposite direction of Arg127 (Supplementary Figure 1B).

3.2. Molecular dynamics simulations and binding free energy via MM-GBSA

In stark contrast to the docking scores, 8 ns molecular dynamics simulations that used the 14 unique docking configurations for each zuonin A enantiomer as a starting point revealed that zuonin A molecules bound to Φ_{hyd} had a lower binding free energy than those bound to S_2 for both enantiomers (Table 2).

Over the course of the MD simulation, the docking predicted that pose **43** of (−)-zuonin A assumed a stable conformation with the tetrahydrofuran ring occupying the φ_A site normally occupied by Leu159 of JIP1 (Fig. 2B). Both methyl groups were on the solvent facing side of the ring in the vicinity of the φ_B recognition site. Visualization of pose **43**'s MD trajectory showed that several key conformational changes in JNK were necessary to achieve this thermodynamically favorable binding mode (Fig. 3B), which occurred within the first ~3 nanoseconds of the simulations. At the beginning of the simulation, one of (−)-zuonin A's 1,3-benzodioxole rings is originally bound to the φ_A–X–φ_B recognition site. Rotation of (−)-zuonin A occurs when the upper 1,3-benzodioxole ring begins to slide past residues Val159, Lys160, Ser161 and Asp162 which create the upper portion of the pocket. These residues are labeled in Fig. 2B. Simultaneously, Glu117-Leu123 undergo a movement in their backbone which creates an induced fit hydrophobic pocket available for tighter binding of the second 1,3-benzodioxole ring. Subsequently, the (−)-zuonin A molecule gets "locked" into place as Arg127 swings upward toward the first 1,3-benzodioxole ring and holds it between its guanidinium cap and the backbone of Asp162 using the side chain of Cys163 as a base.

Decomposing the binding free energy into the contributions from each JNK amino acid reveals several significant interactions, Table 3. One interaction involves the side chain of Val118, −1.787 kcal/mol, which appears to wedge itself between one of (−)-zuonin A's methyls and the 1,3-benzodioxole ring bound to the induced hydrophobic pocket, Fig. 2B. A similar interaction occurs between the backbone of Ser161, −1.361 kcal/mol, and the other side of the THF ring. The residues involved in immobilizing the other 1,3-benzodioxole ring, Arg127, Asp162, and Cys163, all provide major contributions to (−)-zuonin A binding with binding free energies of −1.623, −1.026, and −1.243 kcal/mol, respectively. Other contributions come from the hydrophobic amino acids that line the inside of both the φ_A–X–φ_B recognition site in addition to those that line the induced hydrophobic pocket, Table 3.

The binding free energies calculated for the various (+)-zuonin A trajectories suggest that the (+)-zuonin A enantiomer may also prefer binding to Φ_{hyd}, but in a different fashion. The two poses with the lowest binding energy for (+)-zuonin A were **39** and **46** both of which adopted very similar binding modes. Pose **46** is not shown. The THF ring still primarily occupies the φ_A site, however, unlike with (−)-zuonin A, the two methyl groups point in toward the hydrophobic core and create a small hydrophobic pocket in the same location as the one occupied in the (−)-zuonin A model (Fig. 2A). Unlike, (−)-zuonin A's more dynamic movement, (+)-zuonin A pose **39** stays relatively stationary except for a noticeable dynamic movement of Arg127's side chain which swings down and away from the 1,3-benzodioxole ring of (+)-zuonin A, giving the ring space to lay flat on the peptide backbone of Cys163, Fig. 3A.

The large movement of (−)-zuonin A in the Φ_{hyd} pocket caused it to have a larger standard deviation in its binding free energy (~6 kcal/mol) compared to the other studied poses (~2 kcal/mol), Table 2. The binding free energy of poses **43** for (−)-zuonin A and **39** for (+)-zuonin A in their most stable states (4–8 ns) showed that (−)-zuonin A (−32 kcal/mol) bound to JNK1 with a slightly lower binding free energy than (+)-zuonin A (−30 kcal/mol), supplementary Table 10.

It is to be noted that protein–ligand entropy contributions are not included in these free energy values since current calculation methods are typically time consuming and unreliable. Therefore, the free energy values as presented here represent binding enthalpy and changes in enthalpy during solvation, except the solvent entropy contributions are included via the implicit solvent model. If the protein–ligand entropy contributions to binding between different poses do not vary significantly, the difference in the calculated energy would mostly correlate with the relative binding free energy. This is the main approximation of the MM-GBSA method we are using. Previously we have performed substantial benchmark using this method on a wide range of protein targets and found that for similar ligands of the same protein target, MM-GBSA results indeed provide reasonable correlation with experimental binding free energy [16].

3.3. Comparison to previous (−)-zuonin A binding model

Lastly, it is important to address a previous (−)-zuonin A/JNK interaction study performed by Kaoud et al. [7] which proposed a model of (−)-zuonin binding where the inhibitor was bound to the S_2 region of JNK. Residues that were considered important for (−)-zuonin A binding to the S_2 site were mutated to alanines and kinetic/inhibition assays were performed on the mutants. Of the 5 mutants made (R127A, T164A, W324A, Y130A, C163A) only the R127A mutant led to altered kinetic parameters for c-Jun phosphorylation in the absence of (−)-zuonin A. This data further supports R127's significance in substrate/ligand recognition.

Mutants R127A, C163A and T164A are common to both the S_2 binding pocket and the Φ_{hyd} pocket and provide important binding interactions in both models. The perturbed binding of c-Jun by the R127A mutant makes it difficult to derive any conclusions regarding inhibitor binding, however the IC_{50} values for mutants C163A and T164A both increased by over 1100% and 360% respectively while their maximal inhibition was nearly halved clearly showing that these mutations have some effect on inhibitor binding, which would be expected in either model [7].

An interesting discovery from the previous study was that mutations of the large side chain amino acids Y130 and W324 to alanine in the S_2 binding pocket did not alter c-Jun binding, but increased the percentage inhibition of (−)-zuonin A from 70% when complexed with wild type JNK2 to 95% and 98% when bound to JNK2 mutants Y130A and W324A respectively. Although this result does support the possibility that (−)-zuonin A does indeed bind to the S_2 pocket, one must also consider the long-range effects that these large mutations may have on the entire binding region.

In order to gain further insight and validation into the Φ_{hyd} binding model, it would be beneficial to mutate JNK residues that are predicted to contribute the most to (−)-zuonin binding based on MD simulation data and are unique to the Φ_{hyd} region, such as Val118, Leu123, and Val 159.

Table 2
MM-GBSA results for (−)-zuonin A and (+)-zuonin A complexed with JNK1 after 8 ns MD simulations (kcal/mol). As noted in the text, the free energy is approximate since the protein-ligand entropy contribution was ignored. The gas phase energy was separated into the vdW and electrostatic components. EGB and ESURF are the polar and nonpolar solvation free energies.

Pose #	ΔG binding[a]	ΔG gas			ΔG solv			Docking
	(ΔG gas + ΔG solv)	vdW	EEL	Total	EGB	ESURF	Total	Region
(−)-Zuonin A/JNK1 complex								
43	−26.48 ± 6.36	−32.93	−5.37	−38.30	15.69	−3.87	11.82	Φ_{hyd}
45	−22.22 ± 2.84	−28.25	−2.52	−30.77	12.19	−3.64	8.55	Φ_{hyd}
44	−16.72 ± 2.53	−23.20	0.40	−22.81	8.92	−2.83	6.09	Φ_{hyd}
24	−16.21 ± 2.02	−22.48	−4.68	−27.16	13.61	−2.66	10.94	S_2
33	−15.62 ± 2.28	−22.49	−4.19	−26.67	13.73	−2.68	11.05	S_2
10	−15.39 ± 1.88	−22.36	−4.08	−26.43	13.75	−2.71	11.05	S_2
9	−14.99 ± 2.41	−22.05	−2.96	−25.01	12.66	−2.65	10.01	S_2
31	−14.3 ± 2.19	−20.94	−3.29	−24.23	12.49	−2.56	9.94	S_2
14	−14.04 ± 1.96	−20.78	−2.88	−23.66	12.16	−2.53	9.62	S_2
40	−13.7 ± 1.78	−20.30	−2.84	−23.14	11.94	−2.50	9.44	S_2
37	−13.37 ± 1.87	−19.90	−0.32	−20.22	9.26	−2.41	6.85	S_2
11	−13.29 ± 2.67	−19.28	−2.25	−21.53	10.42	−2.18	8.24	S_2
12	−13.18 ± 2.02	−19.55	−2.36	−21.91	11.04	−2.31	8.73	S_2
27	−12.68 ± 2.31	−18.93	−1.04	−19.98	9.51	−2.21	7.30	S_2
(+)-Zuonin A/JNK1 Complex								
39	−28.92 ± 3.09	−34.56	−3.93	−38.49	13.68	−4.10	9.58	Φ_{hyd}
46	−27.59 ± 3.56	−33.37	−1.76	−35.13	11.45	−3.91	7.54	Φ_{hyd}
49	−25.46 ± 3.00	−31.76	−1.28	−33.03	11.33	−3.76	7.57	Φ_{hyd}
32	−24.21 ± 3.47	−30.65	−1.31	−31.96	11.45	−3.69	7.76	Φ_{hyd}
41	−23.43 ± 2.64	−30.04	−5.49	−35.53	15.74	−3.65	12.09	Φ_{hyd}
34	−16.82 ± 2.49	−23.98	−2.77	−26.75	12.75	−2.82	9.93	S_2
1	−16.81 ± 2.38	−24.04	−3.01	−27.05	13.08	−2.84	10.24	S_2
7	−16.66 ± 2.04	−24.17	−1.09	−25.26	11.39	−2.79	8.60	S_2
19	−16.33 ± 2.27	−23.12	−4.07	−27.20	13.56	−2.69	10.87	S_2
31	−16.20 ± 2.02	−21.98	−3.13	−25.11	11.41	−2.50	8.90	S_2
20	−15.77 ± 2.38	−22.61	−2.43	−25.04	11.99	−2.72	9.27	S_2
15	−15.33 ± 2.34	−21.96	−3.79	−25.75	13.06	−2.63	10.42	S_2
4	−15.23 ± 2.28	−22.31	−2.30	−24.62	11.96	−2.57	9.39	S_2
22	−14.28 ± 1.79	−19.75	−2.08	−21.82	9.87	−2.33	7.54	S_2

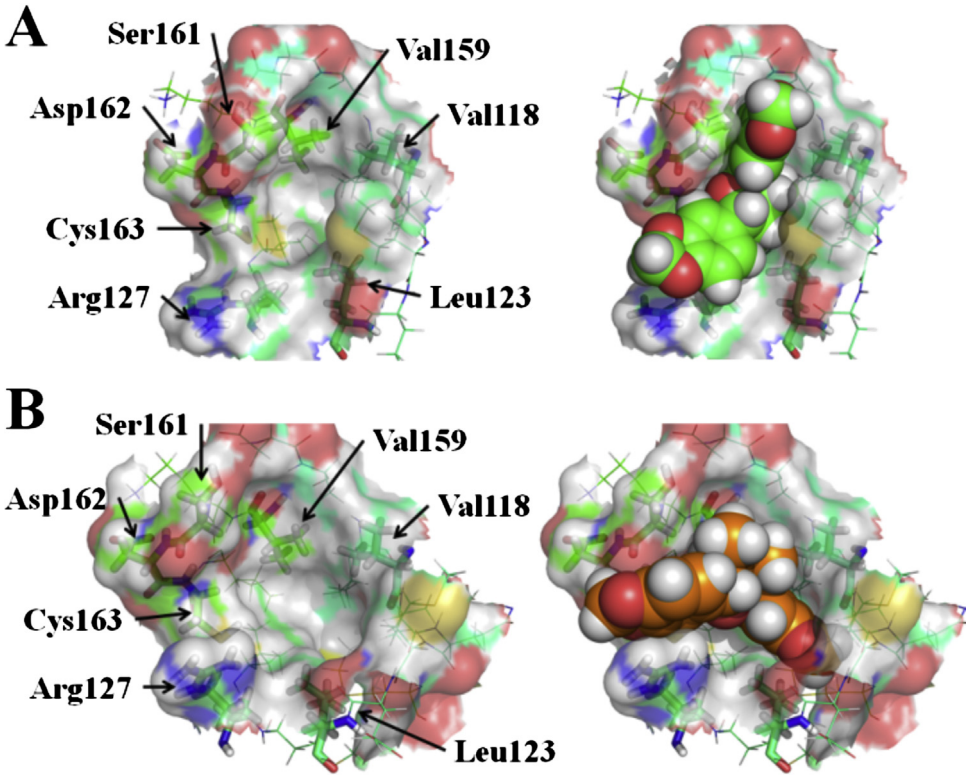

Fig. 2. Stable binding pose of (A) (+)-Zuonin A pose **39** and (B) (−)-Zuonin A pose **43**.

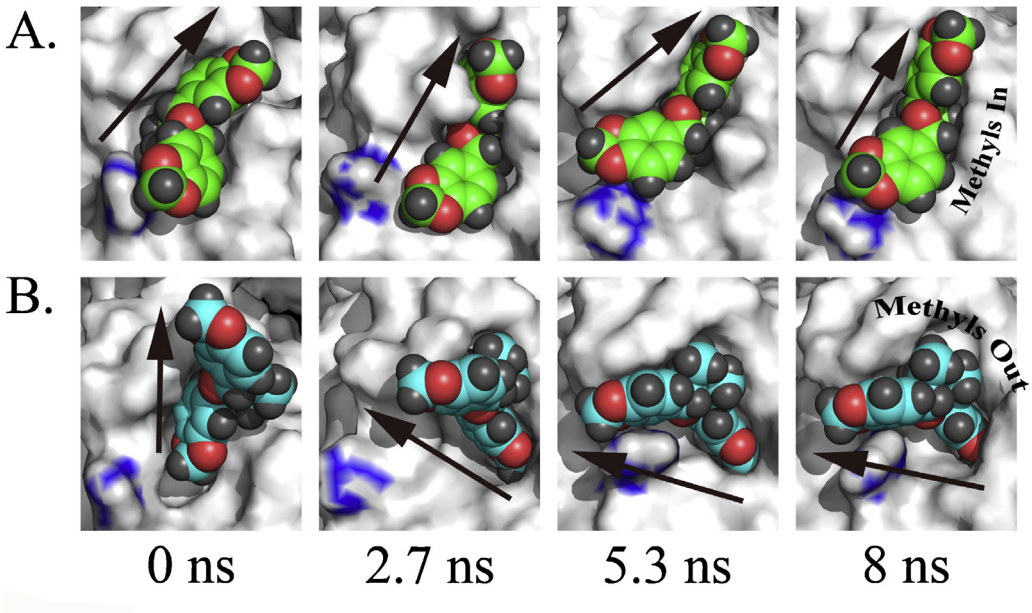

Fig. 3. Trajectory of the "tightest" binding poses, as determined by MM-GBSA calculations, for (A) (+)-zuonin A pose **39**, green, and (B) (−)-zuonin A pose **43**, cyan, with a vector to emphasize the change in orientation. In addition, the location of the methyl groups is specified for each enantiomer. Both are bound to Φ_{hyd} binding site.

Table 3
Contributions of JNK1 residues to the binding of (−)-zuonin A (pose 43) once it has assumed its stable conformation (4–8 ns). All values are in kcal/mol.

(−)-Zuonin A binding energy contributions per JNK1 amino acid								
Residue	Total energy (side chain + backbone)						Side chain	Backbone
	Total	Internal	vdW	Electrostatics	Polar solv.	Non-polar solv.	Total	Total
VAL118	−1.79	0.00	−1.72	−0.40	0.56	−0.24	−1.50	−0.29
ARG127	−1.62	0.00	−2.17	−3.70	4.63	−0.38	−1.58	−0.04
LEU123	−1.45	0.00	−1.36	−0.21	0.30	−0.17	−1.33	−0.12
SER161	−1.36	0.00	−2.13	−0.35	1.48	−0.36	−0.15	−1.21
VAL159	−1.26	0.00	−1.40	0.18	0.08	−0.11	−1.07	−0.19
CYS163	−1.24	0.00	−1.51	0.27	0.14	−0.13	−0.74	−0.51
ASP162	−1.03	0.00	−1.12	−0.18	0.36	−0.09	−0.08	−0.94
LEU131	−1.01	0.00	−0.97	−0.11	0.15	−0.08	−0.96	−0.05
MET121	−0.90	0.00	−0.90	−0.69	0.76	−0.07	−0.44	−0.46
LYS160	−0.90	0.00	−1.06	0.07	0.14	−0.06	−0.02	−0.88
ILE119	−0.84	0.00	−0.86	−0.38	0.43	−0.03	−0.26	−0.58
LEU115	−0.65	0.00	−0.65	0.06	−0.04	−0.02	−0.52	−0.14
MET218	−0.45	0.00	−0.47	−0.12	0.16	−0.01	−0.43	−0.02
ALA113	−0.38	0.00	−0.38	−0.06	0.11	−0.05	−0.27	−0.11
THR164	−0.19	0.00	−0.18	−0.23	0.22	0.00	−0.03	−0.16
LEU165	−0.12	0.00	−0.13	0.03	−0.02	0.00	−0.09	−0.03
GLN120	−0.10	0.00	−0.17	0.05	0.02	0.00	0.00	−0.10

4. Conclusions

Previous work has shown that enantiomers (+)-zuonin A and (−)-zuonin A bind to JNK isoforms with a 100-fold specificity over other MAP kinases and disrupt JNK/substrate interactions at the D-recruitment site (DRS). Although they have a similar affinity for JNK, when bound (−)-zuonin A is a significantly more effective inhibitor of JNK than (+)-zuonin A, reflecting differences in their binding modes.

In this study, molecular docking and molecular dynamics simulations were utilized to examine binding interactions between JNK and both zuonin A enantiomers and to identify differences in their binding modes. First, a series of potential binding pockets and poses were determined using molecular docking along the DRS using the JNK1-pepJIP1 crystal structure as a guide. Each pose was then subjected to molecular dynamics simulations to account for explicit solvent effects and dynamic interactions within the system. The trajectories were then used to estimate the binding free energy for each pose in hopes of discovering the most likely binding interaction. MD simulation results showed that JNK can alter its structure in the presence of either zuonin enantiomer in order to better accommodate binding of the inhibitor.

Although the results of both simulations have both zuonin A enantiomers binding in the same Φ_{hyd} region of JNK1's DRS, they adopt different conformations and have different levels of thermodynamic stability. This difference in the predicted binding pose for each enantiomer may explain why (−)-zuonin A is more effective at inhibiting the phosphorylation of JNK's substrates than (+)-zuonin A.

In addition, the proposed Φ_{hyd} (−)-zuonin A binding model was determined using a different method than that used to describe a previous binding model which suggested that (−)-zuonin A binds to the S_2 binding region. It is possible that these models are not mutually exclusive, but could work in conjunction with one another. To

gain a better insight, it would be beneficial to physically mutate residues that are unique to the Φ_{hyd} pocket and predicted to contribute the largest binding interactions for (−)-zuonin A and note any changes in the effectiveness of zuonin A binding and inhibition.

Acknowledgements

The authors acknowledge the support by the National Institute of General Medical Sciences (R01GM106137 and R01GM59802) and Robert A. Welch Foundation (F-1691 and F-1390).

Appendix A. Supplementary data

Supplementary data associated with this article can be found, in the online version, at http://dx.doi.org/10.1016/j.jmgm.2013.08.008.

References

[1] G.L. Johnson, K. Nakamura, The c-jun kinase/stress-activated pathway: regulation, function and role in human disease, Bba-Mol. Cell Res. 1773 (2007) 1341–1348.
[2] S. Grewal, D.M. Molina, L. Bardwell, Mitogen-activated protein kinase (MAPK)-docking sites in MAPK kinases function as tethers that are crucial for MAPK regulation in vivo, Cell Signal. 18 (2006) 123–134.
[3] C. Davies, C. Tournier, Exploring the function of the JNK (c-Jun N-terminal kinase) signalling pathway in physiological and pathological processes to design novel therapeutic strategies, Biochem. Soc. Trans. 40 (2012) 85–89.
[4] J.S. Heo, S.K. Kim, C.I. Seo, Y.K. Kim, B.J. Sung, H.S. Lee, et al., Structural basis for the selective inhibition of JNK1 by the scaffolding protein JIP1 and SP600125, EMBO J. 23 (2004) 2185–2195.
[5] L.O. Kirkland, C. McInnes, Non-ATP competitive protein kinase inhibitors as anti-tumor therapeutics, Biochem. Pharmacol. 77 (2009) 1561–1571.
[6] T.S. Kaoud, C.L. Yan, S. Mitra, C.C. Tseng, J. Jose, J.M. Taliaferro, et al., From in silico discovery to intracellular activity: targeting JNK–protein interactions with small molecules, ACS Med. Chem. Lett. 3 (2012) 721–725.
[7] T.S. Kaoud, H. Park, S. Mitra, C.L. Yan, C.C. Tseng, Y. Shi, et al., Manipulating JNK signaling with (−)-zuonin A, ACS Chem. Biol. 7 (2012) 1873–1883.
[8] C.L. Yan, T. Kaoud, S.B. Lee, K.N. Dalby, P.Y. Ren, Understanding the specificity of a docking interaction between JNK1 and the scaffolding protein JIP1, J. Phys. Chem. B 115 (2011) 1491–1502.
[9] M.J. Hartshorn, M.L. Verdonk, G. Chessari, S.C. Brewerton, W.T.M. Mooij, P.N. Mortenson, et al., Diverse, high-quality test set for the validation of protein–ligand docking performance, J. Med. Chem. 50 (2007) 726–741.
[10] M.J. Frisch, G.W. Trucks, H.B. Schlegel, G.E. Scuseria, M.A. Robb, J.R. Cheeseman, G. Scalmani, V. Barone, B. Mennucci, G.A. Petersson, H. Nakatsuji, M. Caricato, X. Li, H.P. Hratchian, A.F. Izmaylov, J. Bloino, G. Zheng, J.L. Sonnenberg, M. Hada, M. Ehara, K. Toyota, R. Fukuda, J. Hasegawa, M. Ishida, T. Nakajima, Y. Honda, O. Kitao, H. Nakai, T. Vreven, J.A. Montgomery Jr., J.E. Peralta, F. Ogliaro, M. Bearpark, J.J. Heyd, E. Brothers, K.N. Kudin, V.N. Staroverov, R. Kobayashi, J. Normand, K. Raghavachari, A. Rendell, J.C. Burant, S.S. Iyengar, J. Tomasi, M. Cossi, N. Rega, J.M. Millam, M. Klene, J.E. Knox, J.B. Cross, V. Bakken, C. Adamo, J. Jaramillo, R. Gomperts, R.E. Stratmann, O. Yazyev, A.J. Austin, R. Cammi, C. Pomelli, J.W. Ochterski, R.L. Martin, K. Morokuma, V.G. Zakrzewski, G.A. Voth, P. Salvador, J.J. Dannenberg, S. Dapprich, A.D. Daniels, O. Farkas, J.B. Foresman, J.V. Ortiz, J. Cioslowski, D.J. Fox, Gaussian 09, Gaussian, Inc., Wallingford, CT, 2009.
[11] U.C. Singh, P.A. Kollman, An approach to computing electrostatic charges for molecules, J. Comput. Chem. 5 (1984) 129–145.
[12] B.H. Besler, K.M. Merz, P.A. Kollman, Atomic charges derived from semiempirical methods, J. Comput. Chem. 11 (1990) 431–439.
[13] D.A. Case, T.A. Darden, T.E. Cheatham III, C.L. Simmerling, J. Wang, R.E. Duke, R. Luo, R.C. Walker, W. Zhang, K.M. Merz, B. Roberts, S. Hayik, A. Roitberg, G. Seabra, J. Swails, A.W. Goetz, I. Kolossváry, K.F. Wong, F. Paesani, J. Vanicek, R.M. Wolf, J. Liu, X. Wu, S.R. Brozell, T. Steinbrecher, H. Gohlke, Q. Cai, X. Ye, J. Wang, M.-J. Hsieh, G. Cui, D.R. Roe, D.H. Mathews, M.G. Seetin, R. Salomon-Ferrer, C. Sagui, V. Babin, T. Luchko, S. Gusarov, A. Kovalenko, P.A. Kollman, AMBER 12, University of California, San Francisco, 2012.
[14] U. Essmann, L. Perera, M.L. Berkowitz, T. Darden, H. Lee, L.G. Pedersen, A smooth particle Mesh Ewald method, J. Chem. Phys. 103 (1995) 8577–8593.
[15] G.D. Hawkins, C.J. Cramer, D.G. Truhlar, Pairwise solute descreening of solute charges from a dielectric medium, Chem. Phys. Lett. 246 (1995) 122–129.
[16] T. Yang, J.C. Wu, C. Yan, Y. Wang, R. Luo, M.B. Gonzales, et al., Virtual screening using molecular simulations, Proteins. 79 (2011) 1940–1951.